Beta-MCM-41 micro-mesoporous catalysts in the hydroisomerization of n-heptane: Definition of an indexed isomerization factor as a performance descriptor

Li Gao, Zhiyuan Shi, Ubong Jerome Etim, Pingping Wu, Dezhi Han, Wei Xing, Svetlana Mintova, Peng Bai, Zifeng Yan

Beta-MCM-41 micro-mesoporous catalysts in the hydroisomerization of n-heptane: definition of an indexed isomerization factor as a performance descriptor

Li Gao [a,b], Zhiyuan Shi [c], Ubong Jerome Etim [a], Pingping Wu [a], Dezhi Han [d], Wei Xing [e], Svetlana, Mintova, [a] Peng Bai [a,*], Zifeng Yan [a,*]

[a] State Key Laboratory of Heavy Oil Processing, College of Chemical Engineering, China University of Petroleum (East China), Qingdao, China, 266580

[b] Department of Petrochemical Engineering, Karamay Vocational and Technical College, Xinjiang, China, 833600

[c] Dushanzi Petrochemical Company, Xinjiang, China, 833600

[d] College of Chemical Engineering, Qingdao University of Science and Technology, Qingdao, China, 266042

[e] College of Science, China University of Petroleum (East China), Qingdao, China, 266580

* Corresponding authors. Tel: +86-532-86981296.

E-mail address:baipeng@upc.edu.cn (P. Bai), zfyancat@upc.edu.cn (Z. Yan)

Abstract

Beta-MCM-41(BM) composites consisting of Beta zeolite grown on MCM-41 type mesoporous structure were prepared. The composite materials were used as a support for stabilization of Pt. The Pt containing catalysts (Pt/HBM) were applied in n-heptane hydroisomerization reaction. The Pt/HBM catalysts showed higher n-heptane conversion and higher selectivity to isoheptanes in comparison to pure Beta and MCM-41. The results were explained by the accelerated diffusion of isoheptanes in the Pt/HBM composites, and the high concentration of acid sites with a moderate strength in the composites, which reduced the cracking of reactants and products. Based on the experimental results, an indexed isomerization factor (IIF) was deduced, which is correlated with the physical properties of the supports. The results indicated that the isoheptane yield of the catalysts is strongly dependent on the support (IIF). The general IIF descriptor for predicting the isomerization performance of support materials can provide precise guidance for the design of new micro-mesoporous composites.

Keywords: Indexed isomerization factor; Hydroisomerization; n-heptane; Beta-MCMC-41; Micro-mesoporous composites

1. Introduction

Nowadays, the hydroisomerization of straight-chain paraffins is very important in the oil refining industry, especially in enhancing the gasoline octane number, improving the low-temperature performance of diesel, as well as in the production of lube oils with high viscosity index [1, 2]. Although hydroisomerization of C_4-C_6 fractions is well established[3, 4], there is a need for an efficient catalyst for hydroisomerization of alkanes with longer chains (C_7-C_8 fractions and even higher). Weitkamp and co-workers have made pioneer effort in understanding the effect of the alkane chain length on the hydroisomerization & hydrocracking reactions over various catalysts [5, 6]. A prominent tendency in cracking is the fundamental obstacle in the isomerization of n-alkanes with longer than six carbon atoms.

A variety of catalysts has been studied, including Pt- or Pd-containing mordenite [7, 8], zeolite Beta [8-11], heteropolyacid catalysts [12-14], zeolite Y [15, 16] and SO_4^{2-}/ZrO_2 [17, 18]. Among them, the Pt/mordenite catalyst has been used for C_5/C_6 hydroisomerization at a commercial scale in the production of isoparaffins. It tends to give cracking in the hydroisomerization of C_7 due to the slow diffusion of di- and tri-branched heptane isomers in the unidirectional small micropores [7, 19]. In contrast, zeolite Beta performs better in n-heptane hydroisomerization due to its tri-dimensional pore topology [8, 20-22]. In addition, the reduction of Beta crystallite size would improve diffusion. As a consequence, the nanocrystalline zeolite Beta has exhibited better catalytic performance than micronized crystals in n-heptane hydroisomerization [7]. Moreover, compared with mordenite, the nanosized zeolite Beta cracked 50% of n-

heptane and the other 50% converted to isoheptanes, while the former resulted in a complete cracking of n-heptane. As an alternative solution, the diffusion limitations were potentially reduced or eliminated with the creation of mesopores over zeolitic crystals [23-29]. It is evidenced that the mesopores in zeolite Beta can alleviate the extent of intracrystalline diffusion limitation for n-hexane, consequently contributing to the increased hydroisomerization activity. Moreover, the selectivity to monobranched isomers increases because of the easier desorption of products out of the mesopores. Besides, the micro-mesoporous composites [25-27, 29, 30] showed improved performance in hydroisomerization. The micro-mesoporous composites take the advantages of zeolites, which bear moderate acidity, and also the advantage of mesoporous materials with improved diffusivity of bulky molecules. The secondary mesoporous structure is expected to show improvement in hydroisomerization because of the decline in the product residence time, reducing secondary reactions (cracking included).

Various methods to synthesize micro-mesoporous composite materials have been reported since 1996. A Y-MCM-41 composite was prepared via adding zeolite Y crystals into a MCM-41 synthesis gel [31]. Xia et al reported a two-step crystallization process to prepare ZSM-5-MCM-48 micro-mesoporous materials [32]. A composite material containing zeolite Beta (Beta-MCM-41) was prepared by seeding or post synthesis treatment [33]. A novel method for preparation of MOR-MCM-41 composite was reported, where the mordenite was used as a silica-alumina source [34]. The synthesis procedure involves the treatment of mordenite with a solution containing

hexadecyltrimethyl ammonium bromide (CTAB) and sodium hydroxide; the pH was adjusted by adding HCl.

Despite the preparation of various micro-mesoporous composites, the accurate design to achieve the optimum catalytic performance in the hydroisomerization reactions still remains a challenge. Most importantly, a general descriptor to direct the preparation of these composite materials with appropriate properties for hydroisomerization is needing.

Generally, the isomerization performance is related to the balance between surface acidity and diffusion property of composite materials. The optimum material should consist of mesoporous structure without serious sacrifice of the surface acidity. To this end, we prepared the Beta-MCM-41 composite material by using commercial zeolite Beta as an initial material. The different degree of mesoporosity and acidity in the composite materials was achieved by tuning the concentration of alkali solution used for the treatment. The n-heptane was used as a model compound to evaluate the catalytic performance of the composite material in hydroisomerization reaction. In order to describe the structure-performance relationship, an indexed isomerization factor (IIF) was deduced. By using the IIF, the catalytic performance of the composites in hydroisomerization was evaluated. Based on the experimental results, we concluded that the IIF is an appropriate performance descriptor for hydroisomerization catalysts.

2. Experimental

2.1. Materials

Hexadecyltrimethylammonium bromide (CTAB, 99%), tetraethyl orthosilicate (TEOS, 99%), NaOH (AR grade) and $NaAlO_2$ (AR grade) were purchased from Sinopharm Chemical Reagent Co. Ltd, China. Tetraethylammonium hydroxide solution (TEAOH, 25%) was purchased from Aladdin Industrial Corporation. A commercial zeolite Beta (Si/Al=12.5) was provided by Nankai University Catalyst Co. All reagents were put to use as received with no further purification.

2.2. Materials preparation

2.2.1. Beta-MCM-41 Synthesis

The Beta-MCM-41 composite (BM) was prepared using zeolite Beta as a silica-alumina source according to the previous method described in Ref. [35]. The schematic illustration of the synthesis procedure is shown in Fig. 1. Briefly, zeolite Beta (9.6 g) was dispersed in NaOH solution (72 mL) with three concentrations (1.0, 1.5, and 2.0 M), followed by a 50 minutes stirring at 40 °C. Next, aqueous CTAB solution (74 g; 14 wt %) was added (0.86 mL/min) to the above solution. The mixture was adjusted to pH = 9.6 via dropwise addition of an aqueous Acetic acid (CH_3COOH) solution (50 wt %) under vigorous stirring. After 15 minutes stirring, the mixture was loaded in an autoclave and hydrothermally treated for 48 h at 100 °C. The resulting material was filtered, followed by washing with deionized water, and drying for 12 hours at 100 °C. Finally, the organic template was removed by calcination of the powder samples (12 hours at 550 °C). The samples obtained are named BM (n), where n is representing the concentration of the NaOH solution used in the synthesis.

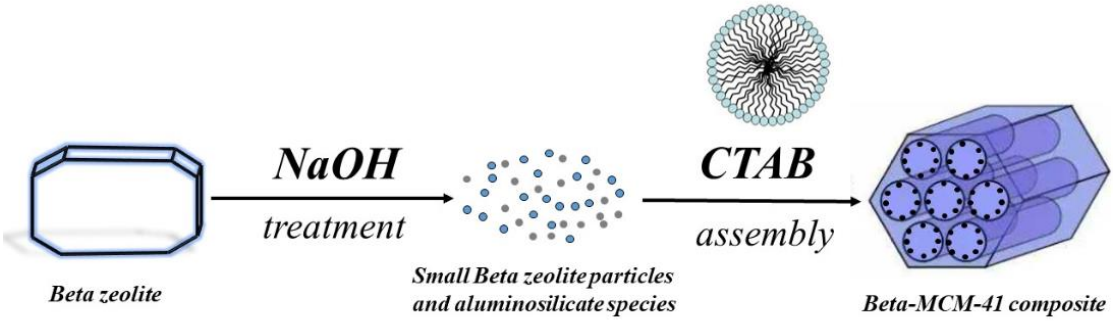

Fig. 1. Schematic illustration of the synthesis procedure of Beta-MCM-41 composite materials.

2.2.2. MCM-41 Synthesis

MCM-41 was synthesized following the procedure described in Ref. [36]. Firstly, CTAB (0.8 g) was mixed with water (39 g) and 2 M NaOH solution (4.0 g). To this solution, TEOS (3.8 g) was added at room temperature, followed by stirring for 30-60 min. The mixture was then placed in an oven for 72 h at 100 °C. After a recovery by filtration, the product was washed by distilled water, followed by drying at 110 ^{o}C, and calcination for 6 h at 550 ^{o}C in air.

2.2.3. Preparation of Beta and MCM-41 physical mixture

A physical mixture of Beta and MCM-41 designated as PBM was prepared as following: Beta (1 g) and MCM-41 (1 g) were added into 8 mL of H_2O, which was then stirred for 4 h at room temperature and dried for 20 h at 50 ^{o}C.

All prepared samples BM, PBM and Beta were ion exchanged with NH_4Cl solution (1.0 M) for 1 h at 80 °C, and finally washed by distilled water. The ion-exchanged products were dried for 3 h at 110 °C and then calcined for 5 h at 550 °C.

The ion exchange procedure was repeated three times in order to obtained the H-form products of the products: HBM, HPBM and HBeta.

2.3. Preparation of catalysts

The Pt was loaded with the same concentration (0.4 wt %) in all samples. The materials (HBM, HPBM, HBeta and MCM-41) were impregnated with an aqueous $H_2PtCl_4 \cdot 6H_2O$ solution. The impregnated materials (catalysts) were dried for 12 h at 110 °C and calcined for 4 h at 400 °C. The catalysts were shaped in pellets, ground and sieved to 40-60 mesh prior to use.

2.4. Catalytic Test

Hydroisomerization of n-heptane was performed on a fixed-bed micro-reactor (see Fig. S1). The stainless tube reactor has a length of 60 cm and a diameter of 0.8 cm. In a typical run, the catalyst (0.5 g; 40-60 mesh) was placed into the reactor. Before reaction, the catalyst was in-situ reduced under a H_2 flow for 4 h at 400 ^oC. The reaction conditions were: atmospheric pressure, temperature of 240 ^oC, weight hourly space velocity of 2.46 h^{-1}, and the H_2/n-heptane molar ratio was 6.0. The effluent mixture were analyzed online with a gas chromatograph (Techcomp GC-7900) equipped with a TM-1 capillary column（50m×0.25mm×0.5μm）and a flame ionization detector (FID).

2.5. Characterization

Powder X-ray diffraction (XRD) was measured using an X'Pert PRO MPD

diffractometer (Philips, Netherland) with a 142 Cu $K\alpha$ radiation (λ = 0.1540 nm) at 40 kV and 40 mA.

Nitrogen sorption isotherms of the samples were recorded using a Micromeritics ASAP 2020 analyzer at -196 ^{o}C. Samples were degassed at 300 ^{o}C before sorption measurements. Surface area was calculated by using the Brunauer-Emmett-Teller (BET) method based on the adsorption data in the relative pressure range of 0.05-0.2 [37]. The meso-pore-size distribution (PSD) was derived from the desorption branch of the isotherm using the Barrett-Joyner-Halenda (BJH) method; the micropores size distribution was evaluated using Horvath-Kawazoe (HK) method.

Fourier transform infrared (FT-IR) spectra were recorded by a Nicolet 6700 spectrometer equipped with a MCT detector and a KBr beam splitter.

Infrared spectra under adsorption of pyridine (Py-IR) were recorded by a NEXUS FT-IR (Thermo Fisher Scientific, 166USA) to stuty the nature of surface acid sites. Before the measurement, samples were degassed for 2 h in vacuum at 573 K to remove the moisture, followed by the pyridine adsorption for 24 h in vacuum. Finally, Py-IR spectra were recorded from 4000 to 400 cm^{-1} using the average record of 64 scans. The quantification of the concentrations of Brønsted (B) and Lewis (L) acid sites can be calculated using C (pyridine on B sites)=1.88IA(B)R^2/W; C (pyridine on L sites) =1.42IA(L)R^2/W described by Emeis [38].

Scanning electron microscopy (SEM) characterization was conducted with a Sirion 200 (FEI) instrument. Transmission electron microscopy (TEM) images were recorded on a JEM-2100 JEOL at 200 kV.

Ammonia temperature programmed desorption (NH_3-TPD) was analyzed on a ChemBET-3000 TPR/TPD (Quantachrome). Typically, 150 mg of sample (20-40 mesh) was pretreated for 1 h at 520 ^oC in a He flow (100 mL min^{-1}) and then cooled to 100 ^oC. After contacting sample with a gas stream of NH_3: He (10.24 vol.% of ammonia; 90 mL min^{-1}) for 10 min, a He flow flushed the sample for 10 min to remove the weakly adsorbed NH_3 molecules. Then the He flow (100 mL min^{-1}) was in contact with the sample with rising of the temperature until 700 ^oC (ramping of 10 ^oC/min).

3. Results

3.1. XRD analysis

XRD patterns of various catalyst supports are presented in Fig. 2. The XRD patterns (5-50^o 2θ) (Fig. 2a) show that zeolite Beta is the only crystalline phase present in all materials [39, 40]. The diffraction peaks corresponding to Beta zeolite in the BM series of samples have relatively low intensity. With increasing the NaOH concentration used for the treatment of Beta zeolite, the intensity of the peaks corresponding to the zeolite phase significantly decreased. In particular, at the concentration of 2.0 M (sample BM(2.0)), the Bragg peaks corresponding to the Beta structure are with very low intensity, while under treatment with a moderate NaOH concentration (1.5 M), the sample BM(1.5) exhibits two distinct peaks of Beta phase. These results indicate that zeolite Beta was destructed after the hydrothermal treatment with the alkaline solution. It was reported that zeolite crystals can be transformed into

smaller particles or even to secondary building units, which can be the source of silicon and aluminum applied for the subsequent assembly of mesostructures [34, 35, 41-43].

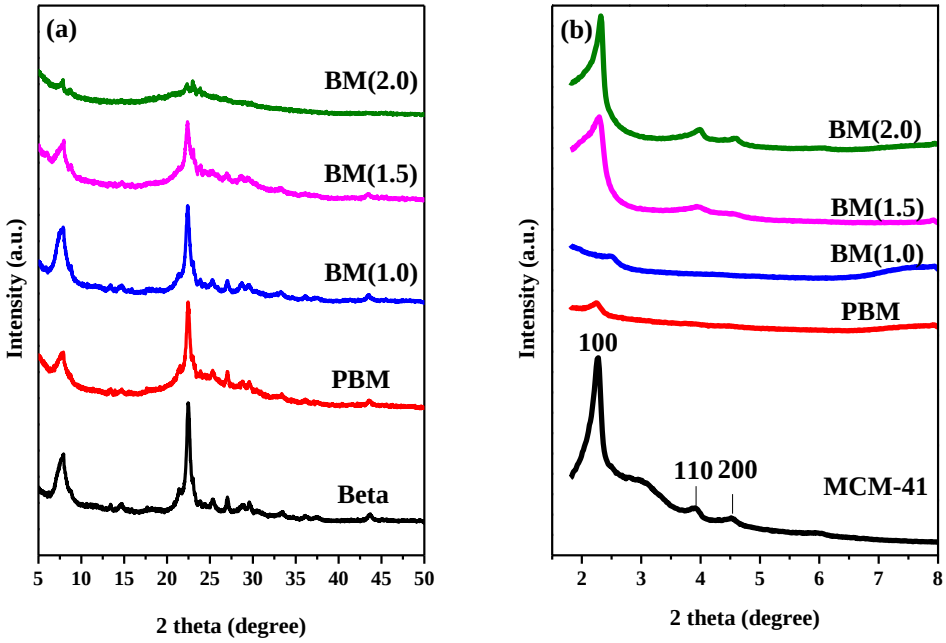

Fig. 2. XRD patterns of catalyst supports in the range (a) 5-50 °2θ and (b) 1-8 °2θ.

On the other hand, the peaks corresponding to the MCM-41 phase can be seen in small-angle XRD patterns of the samples (Fig. 2b). Three peaks corresponding to MCM-41 phase with hkl values of (100) and (110) and (200) measured in the samples [44, 45]. All BM materials display a distinct peak at 2θ of 2.26º with (100) reflection. This peak becomes more pronounced and shifted slightly towards lower angles indicating the development of mesoporous framework in the catalysts supports under treatment with NaOH.

3.2. Pore structure

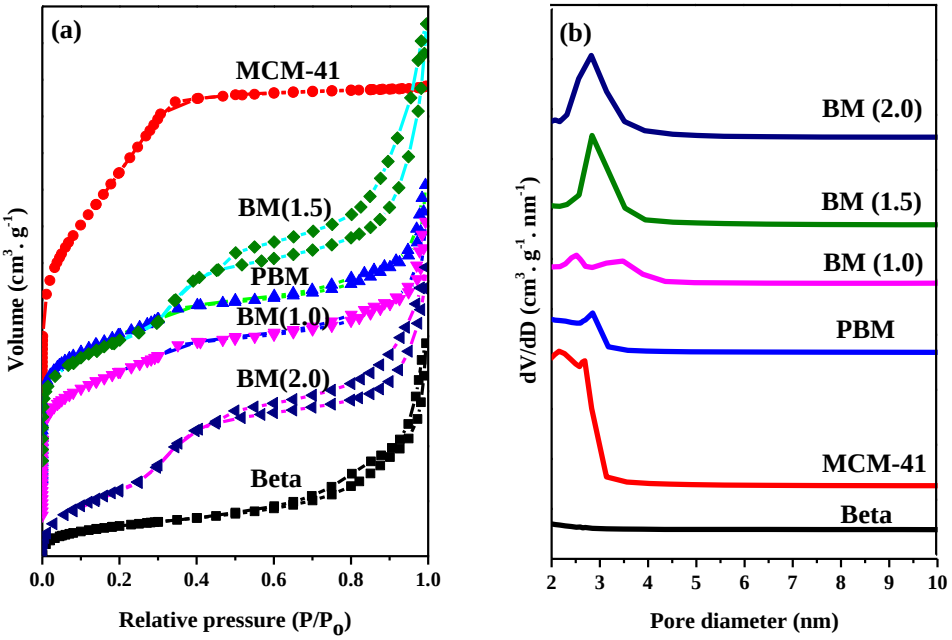

Fig. 3. (a) N_2 adsorption/desorption isotherms and (b) BJH pore size distribution curves of catalyst supports.

N_2 sorption isotherms and the BJH PSD curves of catalyst supports are presented in Figs.3a and 3b, respectively. As can be seen, the N_2 isotherm of MCM-41 contains a small hysteresis loop, which is indicative of mesoporous structure with pores smaller than 4 nm [46]. The isotherm of the parent zeolite Beta corresponds to pure microporous solid. While the composites (BM(1.0), BM(1.5) and BM(2.0)) show both the microporous and mesoporous characteristics, the rise of adsorption amount at the low pressure range below 0.01 corresponds to the filling of zeolite crystalline micropores. Meanwhile, the composite samples exhibit a sharp adsorption step due to the capillary condensation is observed at P/P_0=0.3-0.4, which indicates the existence of ordered

mesoporous structure. The composites display a hysteresis loop ($0.5<P/P_o<1.0$), indicative for the presence of large mesopores or macropores, which is originated by the interparticle spaces [47]. The step at around P/P_0 of 0.4 becomes more pronounced in the samples (BM(1.0), BM(1.5) and BM(2.0)) treated with increased concentration of NaOH. These results are in line with the corresponding XRD data in Fig.2b.

Table 1

Textural properties of catalyst supports.

Samples	S_{BET}[a] (m^2g^{-1})	V_t[b] (cm^3g^{-1})	V_{meso}[c] (cm^3g^{-1})	V_{micro}[d] (cm^3g^{-1})	V_{micro}/V_{meso}	d_{BJH}[e] (nm)	S_{micro}[f] (m^2g^{-1})	S_{meso}[g] (m^2g^{-1})	Crystallinity[h] (%)
Beta	512	0.48	0.17	0.31	1.82	-	397	115	100
MCM-41	1327	0.98	0.91	0.05	0.055	2.69	20	1307	-
PBM	711	0.57	0.29	0.28	0.97	2.83	89	622	-
BM (2.0)	874	0.90	0.78	0.12	0.15	2.78	104	770	92
BM (1.5)	716	0.87	0.67	0.20	0.30	2.84	114	602	79
BM (1.0)	629	0.64	0.38	0.26	0.68	2.49	132	527	41

[a] The total surface area calculated by the BET method.

[b] The total pore volume was obtained at a relative pressure of 0.98.

[c] Mesopore volume calculated using the BJH method.

[d] Micropore volume calculated using the t-plot method.

[e] Mesopore diameter calculated using the BJH method.

[f] Micropore surface area calculated using the t-plot method.

[g] Mesopore surface area calculated using the BJH method.

[h] Relative degree of crystallinity calculated from XRD data.

The bimodal pore distribution in the samples BM(1.0) and MCM-41could be clearly seen (Fig. 3b). Samples BM (2.0), BM (1.5) and PBM have mesopores with a size of 2.8 nm.

Textural and structural properties of catalyst supports are shown in Table 1. As can be seen, MCM-41 and BM possess higher surface areas and larger total pore volumes than that of zeolite Beta. For BM samples, both mesopore volume and mesopore surface area increased with the increase of the NaOH concentration. These findings are consistent with the results of XRD.

3.3. Morphology of catalyst supports treatment with NaOH.

Fig. 4 shows SEM images of the parent Beta, MCM-41, BM(1.5) and PBM. The parent zeolite Beta exhibits discrete particles with sizes in the range of 30-230 nm, which is the typical morphology of zeolite Beta crystals. The PBM (Beta+MCM-41) sample contains a mixture of MCM-41 and zeolite Beta crystals. The large particles are mesoporous MCM-41 with a size less than 1 μm, while the Beta crystals are randomly mixed with the MCM-41. In contrast, the Beta-MCM-41 composite sample BM(1.5) shows a unique morphology, in which, the surface of Beta crystals are with irregular shape and have rough surface. In addition, a layer of either amorphous materials or overgrown MCM-41 material can be seen in the SEM pictures (Fig. 4b). Nevertheless, the two phases were uniformly presented in the samples, which is profoundly different from the physical mixture of zeolite Beta and MCM-41. This could

be explain with dissolution and the re-assembly process occurring within the Beta zeolite crystals under treatment with NaOH.

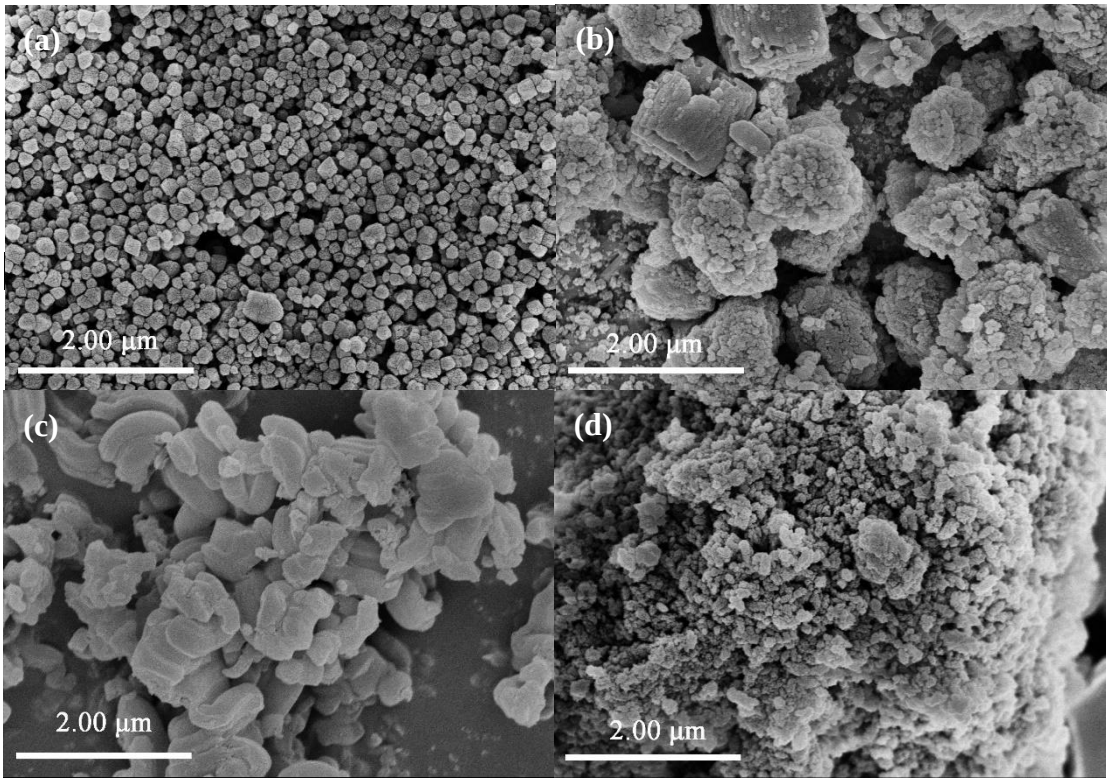

Fig. 4. SEM micrographs of samples (a) Beta, (b) BM(1.5), (c) MCM-41and (d) PBM.

TEM images of MCM-41, BM(1.5) and Pt/BM(1.5) are shown in Fig. 5. MCM-41 contains highly ordered mesopores. TEM images (Fig.5c and d) of sample BM(1.5) contains irregular particles with heterogeneous characteristics, which is suggesting the presence of a mixture. The zeolite nanocrystals of sample BM(1.5) are well dispersed in the mesoporous matrix, rendering them more stable than the nano-sized counterparts. Bagshaw *et al*. [48] reported that the composite samples were made up of (*i*) a crystalline phase, corresponding to the highly stable zeolite Beta, which remains stable during synthesis and post-treatment, and (*ii*) a mesoporous MCM-41, which displays

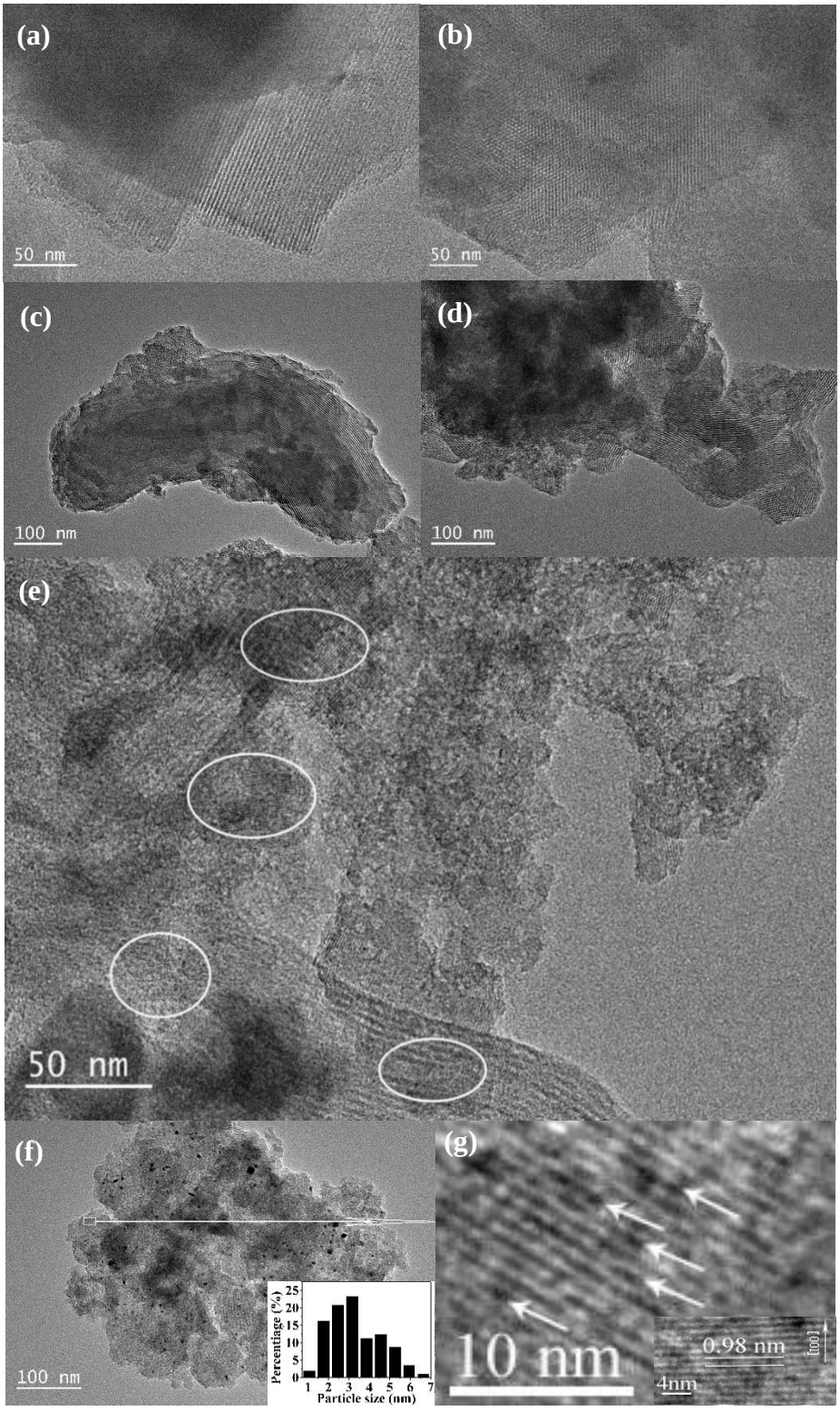

Fig. 5. TEM images of (a-b) MCM-41, (c-e) BM(1.5) composite, and (f-g) Pt/BM(1.5).

poor hydrothermal stability. Consequently, a mesoporous phase is formed via an intra-particle transformation of Beta zeolite under treatment. It can see from Fig. 5e that well-defined Beta crystal lattice fringes orient in different directions and the mesoporous structure overgrew around the Beta crystals. Highly dispersed metallic Pt nanoparticles (NPs) with a size in the range of 1.05-6.65 nm could be observed in the TEM picture (Fig. 5f).

3.4. FT-IR spectra of the supports

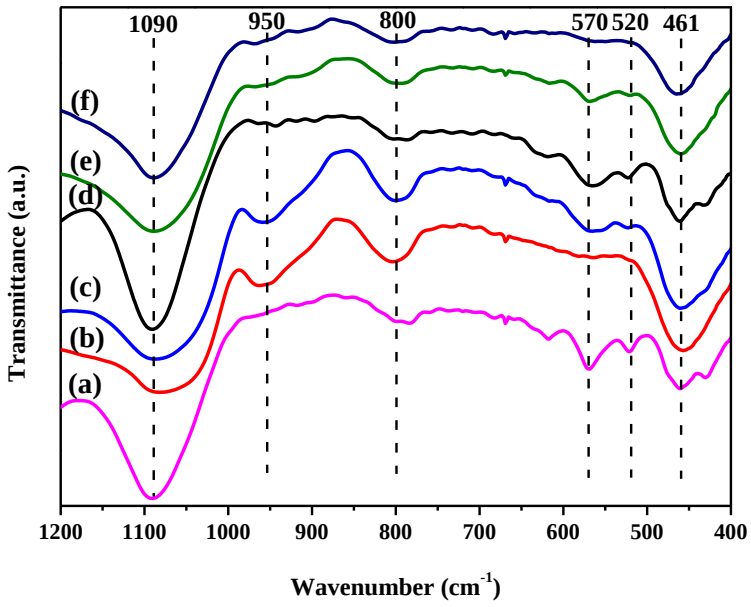

Fig. 6. FT-IR spectra of catalyst supports: (a)Beta, (b) PBM, (c) BM(1.0), (d) BM(1.5), (e) BM(2.0), and (f) MCM-41.

Fig. 6 shows the FT-IR spectra of the catalyst supports. Similar to MCM-41, the framework vibration spectra of BM samples display bands centered at 461, 800, 950

and 1090 cm^{-1}. The band at 461 cm^{-1} is attributed to the Si-O-Si bending vibrations, the band at 800 cm^{-1} to the Si-O-Si symmetric stretching vibrations, and the band at 1090 cm^{-1} to the Si-O-Si asymmetric stretching vibrations. The band at 950 cm^{-1} is assigned to defective Si-OH groups [49]. There are two bands centered at 520 and 570 cm^{-1} in the FT-IR spectra of BM- and Beta samples, which are representative for six- or five-membered rings of T-O-T (T=Si or Al) vibrations of zeolite Beta [50], implying that zeolite Beta is preserved in the BM materials.

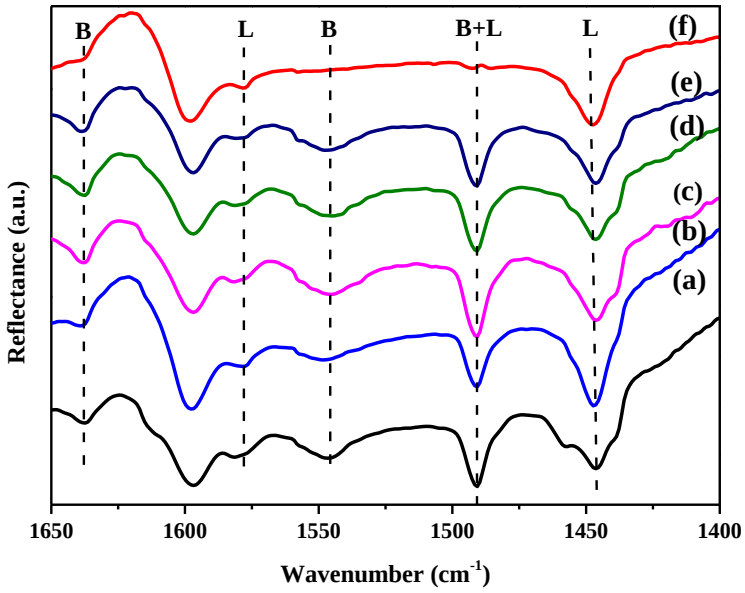

Fig. 7. IR spectra of catalyst supports under pyridine adsorption: (a) HBeta, (b) HPBM, (c) HBM(1.0), (d) HBM(1.5), (e) HBM(2.0), and (f) MCM-41.

IR spectra under adsorption of pyridine were collected from the samples in order to study the acidity of the supports (Fig.7). The bands at 1545 and 1638 cm^{-1} correspond to pyridine adsorbed on B acid sites, while the band at 1490 cm^{-1} is attributed to pyridine

interacting with both B and L acid Sites. The bands at 1450, 1578 cm^{-1} are signature of pyridine adsorbed on the Lewis acid sites [51-53]. The MCM-41 support exhibits signals owning to pyridine adsorbed on Lewis (L) acid sites (bands at 1450, and 1578cm^{-1}) [54]. No Brønsted (B) acid sites in the spectra of the MCM-41support are observed (no band at 1545 cm^{-1}). While the bands at 1545 and 1638 cm^{-1} are present in the spectra of HBeta, HBM, and HPBM catalysts, which are characteristic of the B acid sites. The results indicate that the HBM supports displays an acidity, which resembles that of the HBeta, but differs from the acidity of the MCM-41 support. It is probably explained by that both the HBeta and the HBM supports own zeolite framework aluminum species, which are the base of the B acid sites. As shown in Table 2, for HBM supports (HBM(1.0), HBM(1.5) and HBM(2.0)) have the higher ratio of B/L acid sites. With intensive treatment of the samples by highly concentrated NaOH, the ratio of B/L acid sites decreased.

Table 2

Acidity of samples determined by IR spectroscopy using pyridine as a probe molecule.

Supports	L acid (μmol/g)	B acid (μmol/g)	B/L
HBeta	30	78	2.6
HPBM	43	38	0.9
HBM(2.0)	52	36	0.7
HBM(1.5)	42	41	1.0
HBM(1.0)	25	54	2.1
MCM-41	124	0	0

3.5. NH_3-TPD analysis

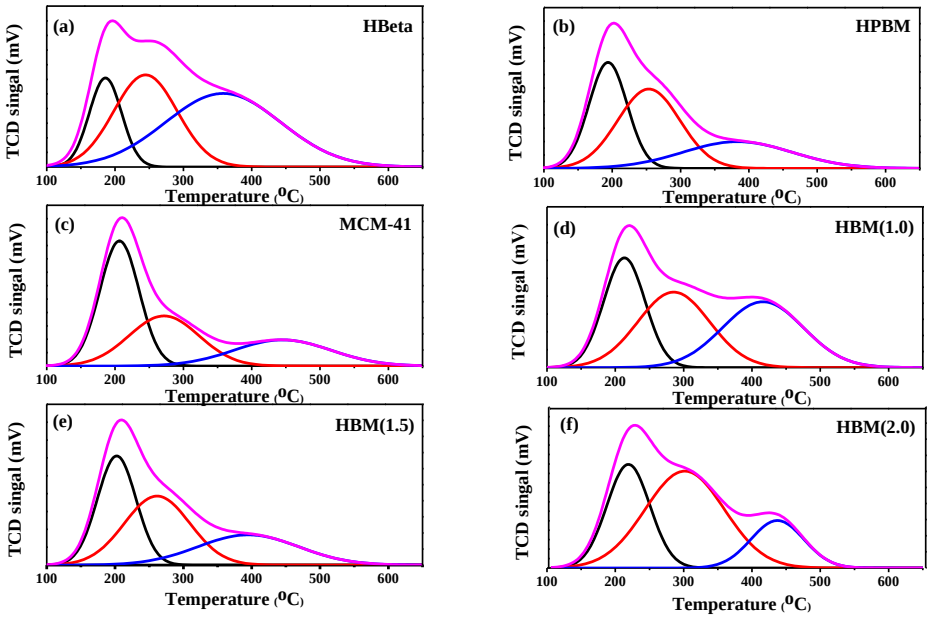

Fig. 8. NH_3-TPD profiles of supports (a) HBeta, (b) HPBM, (c) MCM-41, (d) HBM (1.0), (e) HBM(1.5) and HBM(2.0).

Besides the acidic properties (acid concentration and strength distribution) of the catalysts were characterized by NH_3-TPD. From the ammonia desorption profile based on the desorption temperatures, the acid strength was graded as weak, moderate and strong [55, 56]. Fig. 8 shows the NH_3-TPD profiles of the catalysts. All samples exhibit three peaks in the range of 100-650 ^oC. The peak below 250 ^oC was assigned to the desorption of ammonia weakly adsorbed on the acid sites. The one located in the range of 250-400 ^oC was assigned to the desorption of ammonia moderately adsorbed on the acid sites. The high temperature peak was observed at about 400 ^oC that corresponds to

the strong acid sites. The concentration and strength of acid sites on different samples are summarized in Table 3. Evidently, the HBeta supports has the highest concentration of strong acid sites among all other samples. The concentration and strength of acid sites in HBM sample are generally higher than those in the MCM-41, while are lower than those in the HBeta. For the HBM series, the concentration and strength of acid sites gradually decreased in the order: HBM (1.0) > HBM (1.5) > HBM (2.0).

4. Catalytic performance of catalysts in hydroisomerization of n-heptane

4.1. Catalytic activity

Table 3

Acidity properties of samples determined by NH_3-TPD.

Samples	A_T (μmol/g) [a]	Aw (μmol/g)	A_M (μmol/g)	A_S (μmol/g)
HBeta	68.64	11.50	23.32	33.82
HPBM	55.04	18.04	22.01	14.99
MCM-41	47.92	35.67	8.78	3.47
HBM(2.0)	48.97	14.9	25.68	8.39
HBM(1.5)	57.16	20.13	21.51	15.47
HBM(1.0)	62.84	19.85	23.71	20.28

[a] A_T: Concentration of total acid sites; A_W: Concentration of weak acid sites; A_M: Concentration of medium acid sites; A_S: Concentration of strong acid sites.

The catalytic performance of the catalysts (Pt/HBeta, Pt/HBM(1.0), Pt/HBM(1.5), Pt/HBM(2.0), Pt/HPBM and Pt/MCMC-41) in the n-heptane hydroisomerization was

evaluated (Table 4). Pt/HBeta displayed the highest n-heptane conversion of 81.68% due to the strong acid sites. While the conversion decreased for the catalyst prepared by physical mixing of the two phases (Beta and MCM-41) or by hydrothermal treatment (Beta-MCM-41), samples Pt/HBM(2.0), Pt/HBM(1.5) and Pt/HBM(1.0) showed n-heptane conversions of 20.34%, 55.76% and 60.49%, respectively. A relatively lower conversion (42.18%) was measured over the Pt/HPBM catalyst. The MCM-41 supported catalyst exhibited the lowest conversion (0.765%) among all catalysts.

4.2. Isomerization selectivity

Over the catalysts, various C_7 isomers have been identified as products, for examples, 2-methylhexane, 3-methylhexane, 3-ethylpentane, 2,2-dimethylpentane, 2,3-dimethylpentane, 2,4-dimethylpentane, 3,3-dimethylpentane and 2,2,3-trimethylbutane. In the monobranched C_7 isomers, 3-methylhexane is predominant because more protonated cyclopropane intermediates can be transformed into 3-methylhexane instead of into 2-methylhexane; 3-methylhexane is expected to be produced mainly on solids, on which no steric restrictions exist [16]. The selectivity of the catalysts in correspondence to different kinds of product lumps (such as monobranched, multibranched, or cracking products) are shown in Table 4. Among all samples, the Pt/HBeta showed the lowest selectivity to isomerization products (41.34%). A comparable low selectivity of 42.43% was observed over the Pt/HPBM catalyst. In terms of Pt/HBM sample, the selectivity towards isoheptane products was enhanced for samples (Pt/HBM(1.0), Pt/HBM(1.5) and Pt/HBM(2.0)). Consequently,

Table 4

Catalytic results of samples in the hydroisomerization of n-heptane.

	Pt/HBeta	Pt/HBM(1.0)	Pt/HBM(1.5)	Pt/HBM(2.0)	Pt/HPBM	Pt/MCM-41
Propane	20.61	6.13	1.83	0.82	10.21	0
Iso-butane	27.30	11.93	5.92	1.13	14.07	0
2-methylhexane	12.84	13.41	15.83	7.51	6.90	0.23
3-methylhexane	10.88	16.54	17.65	8.11	7.62	0.31
3-ethylpentane	0.82	0.85	1.65	0.37	0.32	0.13
2,2- dimethylpentane	1.91	1.76	1.82	0.27	0.41	0
2,3- dimethylpentane	3.39	4.40	4.65	1.18	1.29	0.09
2,4- dimethylpentane	2.96	4.06	4.34	0.84	1.19	0
3,3- dimethylpentane	0.74	0.77	1.27	0.09	0.13	0
2,2,3- trimethylbutane	0.23	0.64	0.80	0.02	0.04	0
Conversion (%)	81.68	60.49	55.76	20.34	42.18	0.77
Mono-isoheptane yield (%)	24.54	30.8	35.13	15.99	12.84	0.67
Multi-isoheptane yield (%)	9.23	11.63	12.88	2.40	3.06	0.095
Isomer selectivity (%)	41.34	70.14	86.11	90.41	42.43	100.00
Yield (%)	33.77	42.43	48.01	18.39	17.90	0.77
Cracking selectivity (%)	58.66	29.86	13.89	9.59	57.57	0

Reaction conditions: temperature: 240 ^{o}C; WHSV: 2.46 h^{-1}; pressure: 1 atm; H_2/n-heptane (mole)=6; reaction time on stream: 240min.

the Pt/HBM(2.0) exhibited much higher selectivity (90.41%), while the Pt/HBM(1.5) and the Pt/HBM(1.0) showed moderate selectivity of 86.11% and 70.14%, respectively. In comparison to the Pt/HPBM, the Pt/HBM sample has higher selectivity to isomerization products coupled with a significantly high conversion. It is due to the

high portion of MCM-41 structured mesopores in the BM composite (BM(1.0), BM(1.5) and BM(2.0)) connected with the micropores of zeolite Beta [57], which is not observed in the Pt/HPBM catalyst. Compared with the Pt/HBeta catalyst, the Pt/HBM shows higher selectivity to the di-branched C_7 isomers with the following sequence: 2,3-dimethylpentane>2,4-dimethylpentane>2,2-dimethylpentane>3,3-dimethylpentane. The di-branched C_7 isomers obtained over the Pt/HBM catalyst is derived from secondary skeleton isomerization of 3-methylhexane and 2-methylhexane [58]. Besides, the Pt/HBM samples exhibited much lower selectivity to cracking products, and the main cracking products were propane and isobutane (Table 4). Only trace amounts of n-butane was detected, which is consistent with the previous reported results [59]. This is due to the cracking of 2,2-dimethylpentane and 2,4-dimethylpentane which usually proceeds through β- session reactions, and not direct cracking of n-C_7 [60-66], leading to the formation of iso-butane and propane.

5. Discussion

5.1. Effect of pore structure of supports on catalysts selectivity towards isoheptanes

The selectivity of catalysts to isomerization products depends strongly on channel structure, geometry and structural regularity of support materials [67, 68]. The relationship between isoheptanes selectivity and the mesopore volume of the supports is shown in Fig.9. Surprisingly, for all catalysts, the selectivity to isoheptanes shows a nice positive correlation with the mesopore volume of the support materials. Higher

mesopore volume leads to a higher isomerization selectivity. That is due to the enhanced diffusion in the samples. The transport efficiency of molecules in micro-composite materials is more efficient than that of purely microporous materials[69]. This has been unequivocally verified by the diffusion experiment with neopentane in mesoporous ZSM-5 zeolite [70]. The shorter diffusion path length in the materials decreases the residence time of carbocationic intermediates on the acid sites, thus suppressing their further cracking [71]. Therefore, micro-mesoporous composite materials exhibit a higher isomerization selectivity compared with the pure microporous materials [72].

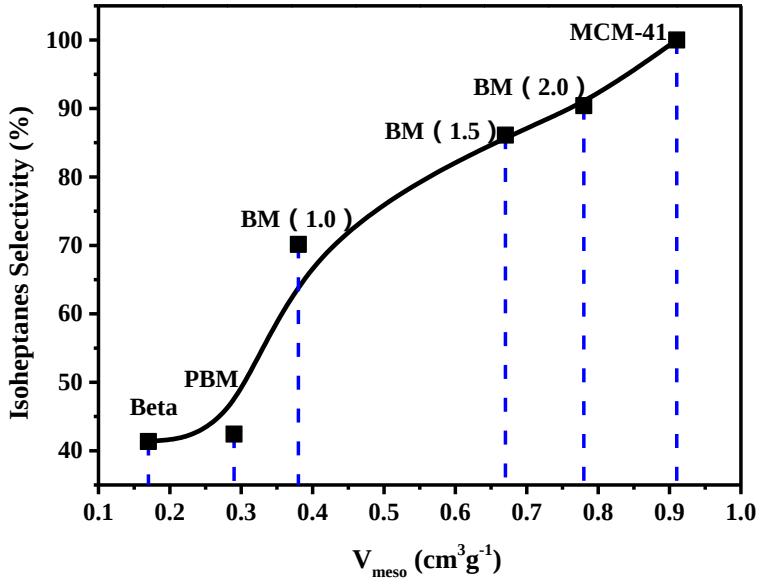

Fig. 9. Isoheptanes selectivity as a function of mesopore volume of support samples (Beta, PBM, BM(1.0), BM(1.5), BM(2.0) and MCM-41).

5.2. Effect of support acidity on the conversion of catalysts in the hydroisomerization of n-heptane

In hydroisomerization, the strength and concentration of acidic sites play an important role [73]. Generally, alkane conversion depends largely on zeolite acidity [68, 74]. On one hand, the hydroisomerization activity of catalysts increases with the concentration of acid sites [74, 75]. As shown in Fig. 10a, the conversion of catalysts exhibits a positive correlation with the concentration of total acid sites of the supports. The Pt/HBeta catalyst showed the highest n-heptane conversion (81.86%) because of the greater concentration of acid sites. In the Pt/HBM, a decrease of the concentration of acid sites, and especially the strong acid sites [76, 77], resulting in a lower conversion to isomerization was observed. The Pt/MCM-41 catalyst displayed a much lower conversion compared with that of the Pt/HBM catalysts (Pt/HBM(1.0), Pt/HBM(1.5) and Pt/HBM(2.0)), even though it had higher surface area and larger pore volume. It might be explained by the weaker acidity of the pure silicon MCM-41.

On the other hand, the catalytic activities of the samples also display strong relation with the acid strength of the zeolites [75, 78], which can be qualitatively identified with the location of peaks in the TPD profile. The catalytic activity for n-heptane conversion decreased in the order of Pt/HBeta > Pt/HBM(1.0) > Pt/HBM(1.5) > Pt/HPBM > Pt/HBM(2.0) > Pt/MCM-41 (Table 4). Correlating the results shown in Fig. 9, Fig.10b and Table 3, it is shown that the n-heptane conversion of the catalyst (Pt/HBeta, Pt/HBM(1.0), Pt/HBM(1.5), Pt/HBM(2.0), Pt/HPBM and Pt/MCMC-41)

exhibits a strong positive dependency on the acid strength of supports. This can be explained that high acid sites beneficial for decreasing the activation energy in the rate-limiting step and enhancing the conversion activity [74], which afforded a longer residence time for the carbenium intermediates [73, 75]; The latter intermediates are isomerized further [77].

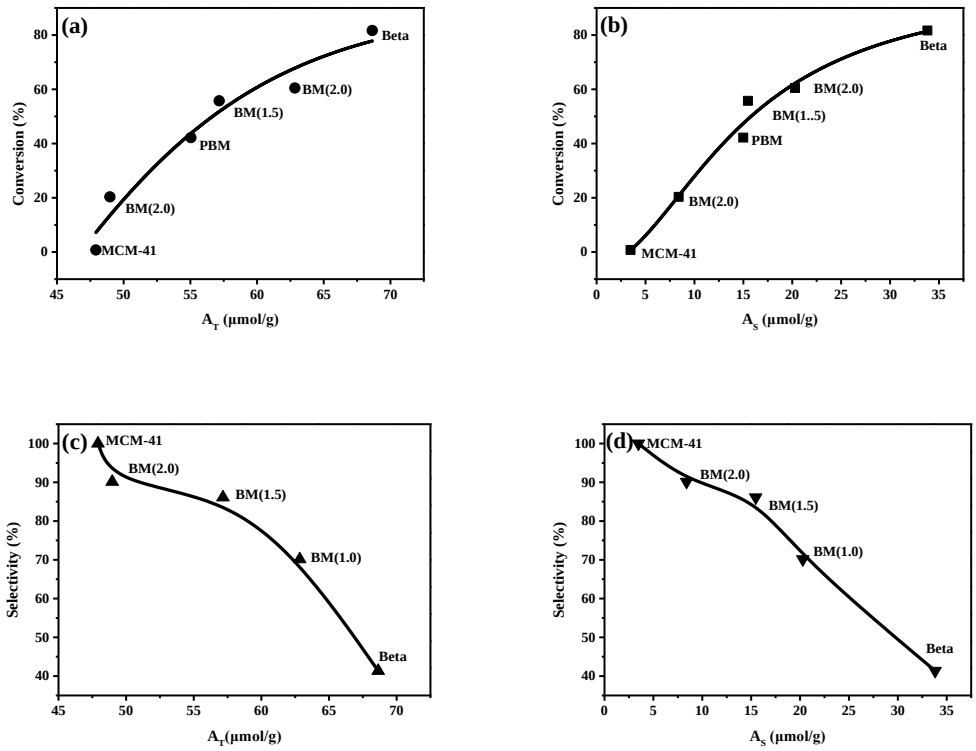

Fig. 10. N-heptane conversion (a-b) and isoheptane selectivity (c-d) of catalysts as a function of support A_T and A_S.

5.3. Effect of support acidity on the isoheptane selectivity

Selectivity towards heptane isomers depends on various factors including the structure and acidity of the catalyst [64]. It was found that catalysts possessing higher

concentration of acidic sites exhibited a lower isomer selectivity due to cracking product formation [73]. Increasing the concentration of acid sites enhances the chance of isoalkene intermediates to interact with acidic sites and the cracking is boosted [75, 79]. Therefore, isoheptane selectivity is decreased. In addition to the acidic site concentration, acid strength is another important factor of the selectivity. Higher acid strength guarantees a relatively longer holding time of the carbenium intermediates on the acid sites, allowing for the intermediates to be cracked [73, 75, 77]. Fig. 10c and Fig. 10d show the relationship between the isomerization selectivity and concentration and strength of support acid sites, respectively. As can be seen from Fig. 10c and Fig.10d, the concentration of total acid sites and the concentration of strong acid sites followed the reverse sequence as selectivity. In detail, the isomerization selectivity of the catalysts decreased in the following order: Pt/HBeta < Pt/HBM(1.0) < Pt/HBM(1.5) < Pt/HBM(2.0) < Pt/MCM-41. While the concentration of total acid sites and the concentration of strong acid sites increased as follow: HBeta > HBM(1.0) > HBM(1.5) > HBM(2.0) > MCM-41. In the Pt/HBeta, the higher concentration and stronger acid centers led to the formation of more cracked products, and thus, a reduced hydroisomerization selectivity [73]. On the other hand, moderate concentration of total acid sites and acid strength of the Pt/HBM benefit the skeletal isomerization, because too strong acidity generally favors cracking, while weak acidity leads to a low activity [80]. In conclusion, the higher concentration of strong acid sites induces significant cracking reactions [55, 77, 81, 82], which explains the much higher isomerization selectivity observed in the HBM series samples than in the sample containing pure

zeolite Beta.

5.4. General descriptor for evaluation of catalysts performance: *indexed isomerization factor (IIF)*

Table 5

Properties of supports.

supports	A_T [a] (μmol/g)	$A_T/A_{T,max}$ [b]	A_S [c](μmol/g)	$A_S/A_{S,max}$ [d]	support	V_{meso}(cm^3/g)	$V_{meso}/V_{meso,max}$ [e]	IIF[f]
HBeta	68.64	1.00	33.82	1.00	Beta	0.17	0.19	0.19
HPBM	55.04	0.80	14.99	0.44	PBM	0.29	0.32	0.11
HBM(1.0)	62.84	0.92	20.28	0.60	BM(1.0)	0.38	0.42	0.23
HBM(1.5)	57.16	0.83	15.47	0.46	BM(1.5)	0.67	0.74	0.28
HBM(2.0)	48.97	0.71	8.39	0.25	BM(2.0)	0.78	0.86	0.15
MCM-41	47.92	0.70	3.47	0.10	MCM-41	0.91	1.00	0.07

a Concentration of total acid sites calculated using NH_3-TPD

b Concentration of strong acid sites calculated using NH_3-TPD

c Relative concentration of total acid sites calculated using the concentration of total acid sites with respect to their maximum value

d Relative concentration of strong acid sites calculated using the concentration of strong acid sites with respect to their maximum value

e Relative mesopore volume calculated using mesopore volume with respect to their maximum value

f Calculated as $(V_{meso}/V_{meso,\ max})\times(A_T/A_{T,\ max})\times(A_S/A_{S,\ max})$

The above discussion clearly indicates that the catalytic performance of catalysts is closely related to the physical properties of support materials, such as mesopore volume, concentration of acid sites, and concentration of strong acid sites. These factors

act somehow competing. A large mesopore volume is favorable to achieve a high isoheptane selectivity, while a high concentration of acid sites, especially the strong acid sites, enhances the heptane conversion, but decrease isomerization selectivity. Although similar findings have been observed before, [73, 75, 77], there is no a general descriptor that can be used to evaluate the performance of a catalyst based on the physical properties of support materials.

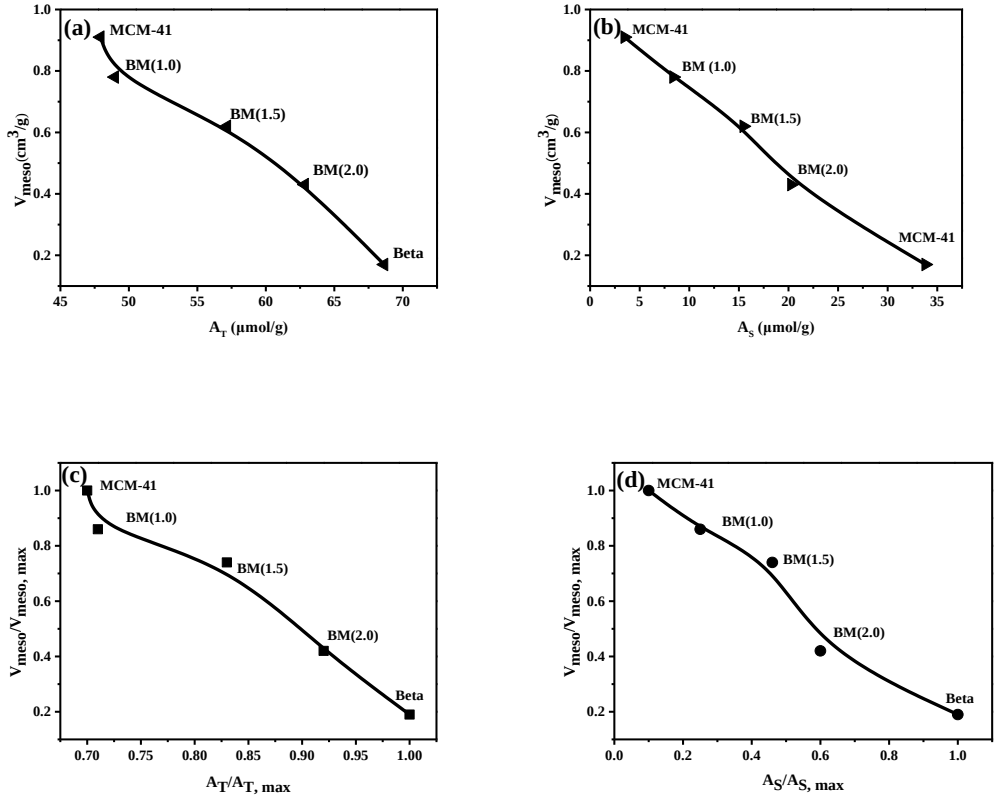

Fig. 11. Mesopore volume as a function of the concentration of total acid sites (a), concentration of strong acid sites (b) and the relative mesopore volume as a function of relative concentration of total acid sites (c) and the relative concentration of strong acid sites (d).

The results above show that on one hand, the acidity of the supports is closely related to the mesopore volume. As can be seen in Fig. 11a and Fig. 11b, the acidity shows a negative correlation with the mesopore volume. In other words, the mesopore formation by the recrystallization process in the supports is accompanied by an evident decrease of the acidity and an increase of the mesopore volume. To be more specific, the A_T decreases from 68.64 μmol/g in Beta to 48.97 μmol/g in BM(2.0), and the A_S decreases from 33.82 μmol/g in Beta to 8.39 μmol/g in BM(2.0), while the mesopore volume increases from 0.17 cm^3/g in Beta to 0.78cm^3/g in BM(2.0). It means that the mesoporous volume increases by about five folds, while sacrificing 30% of the concentration of total acid sites and 75% of the concentration of strong acid sites. The V_{meso}, $A_{T,}$ and A_S were normalized with respect to their maximum values, thus the relative mesopore volume ($V_{meso}/V_{meso,\ max}$), relative concentration of total acid sites ($A_T/A_{T,\ max}$) and relative concentration of strong acid sites ($A_S/A_{S,\ max}$) were obtained. As shown in Fig.11c and Fig.11d, there is also a similar relationship between relative concentration of acid sites ($A_S/A_{S,\ max}$, $A_T/A_{T,\ max}$) and relative mesopore volume ($V_{meso}/V_{meso,\ max}$). By combining the above relative values with the catalytic performance of catalysts, a clear relationship was observed between the physical properties (acidity, mesopore volume) of supports and the isoheptanes yield of catalysts. Therefore, an indexed isomerization factor (IIF) as a function of the relative mesopore volume ($V_{meso}/V_{meso,\ max}$), the relative concentration of total acid sites ($A_T/A_{T,\ max}$) and the relative concentration of strong acid sites ($A_S/A_{S,\ max}$) of supports was proposed as

follows: $IIF = (\frac{V_{meso}}{V_{meso,\max}}) \times (\frac{A_T}{A_{T,\max}}) \times (\frac{A_S}{A_{S,\max}})$. By using the IIF, the effect of the physical properties of supports on the isoheptanes yield of catalyst was evaluated.

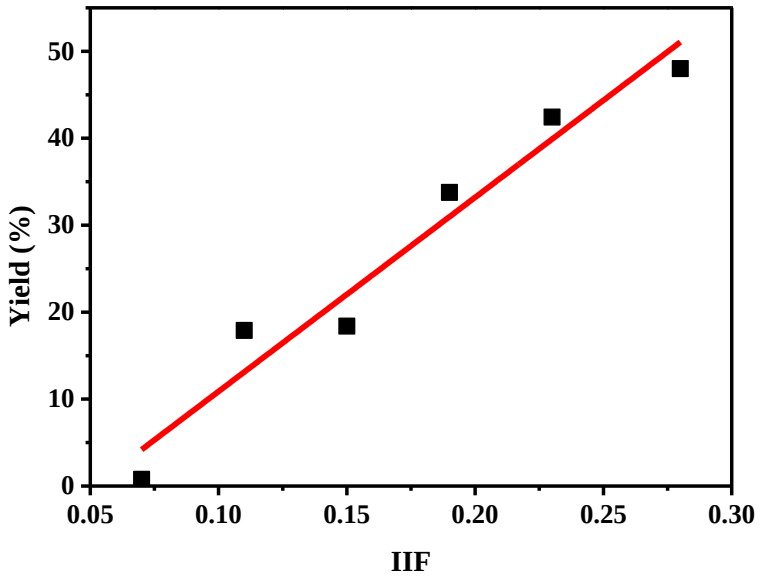

Fig. 12. The correlation between IIF and the isoheptane yield of catalysts.

The detailed fitting process are provide in Supplementary Information. Linear fitting formula, parameters of linear fitting and linear fitted curves are displayed in Equation S1, Table S1 and Fig.S2 respectively. The isoheptane yields of the materials show a clear positive correlation with the IIF (Fig. 12, and Table 5). It implies that the IIF could be applied to predict the isoheptane yield of a catalyst. As can be seen, the IIF of the BM(1.5) samples (0.28) is much higher than that of the microporous zeolite Beta (0.19) because the former possesses superior diffusion properties. For the BM(1.5) sample, the decrease of the acidity is not so pronounced as the increase of the mesopore volume. Thus, this sample bears a high diffusion efficiency together with an appropriate

amount of acid sites, achieving a superior overall catalytic performance. BM(2.0) exhibits a much lower IIF (0.15), because the introduction of mesopores in the zeolite results in serious loss of acidity, resulting in a decrease of the catalytic activity. Compared to the BM (1.5) catalyst, the IIF (0.23) for BM(1.0) was slightly lower, which is due to the lower mesopore volume, resulting in the slow diffusion rate of the isomerized intermediates and products. Although the MCM-41 has a large mesopore volume, it has the weakest acidity, giving the lowest IIF (0.07) of isoheptanes among all catalysts. For the sample with a physical mixture of Beta and MCM-41 (sample PBM), a poor balance between acidity and mesopore volume renders a low IIF (0.11), resulting in a low isoheptane yield.

6. Conclusion

In this study, Beta-MCM-41 materials were hydrothermally synthesized and applied as supports for the preparation of bifunctional catalysts (Pt/HBM) for n-heptane hydroisomerization. The Pt/HBM(1.5) and Pt/HBM(1.0) catalysts are superior than the pure Beta and the physical mixture of HBeta and MCM-41. As a result, sample Pt/HBM(1.5) displays high selectivity to isomerization (86.11%) together with a relatively high conversion (55.76%) of n-heptane, achieving the highest yield (48.01%) of isoheptanes among all samples. By correlating the catalytic performance with the physical properties of catalysts, it was found that the superior performance of the micro-mesoporous composite is attributed to the superior mass transport of large isoheptane molecules in the micro-mesoporous architecture and the high proportion of moderate

strength acid sites in the catalyst, which suppresses the cracking reactions. These results indicate that the Pt/HBM(1.5) catalyst is a potential candidate for the hydroisomerization of n-heptane. In order to predict the isomerization performance and provide rational guidance for the design of support materials, an indexed isomerization factor was deduced and used as a general performance descriptor for isomerization catalysts.

Acknowledgements

This work was financially supported by the National Key Research and Development Program of China (2017YFB030660), the Joint Funds of the National Natural Science Foundation of China and China National Petroleum Corporation (U1362202), Natural Science Foundation of China (51601223, 21206195, U1510109), the Fundamental Research Funds for the Central Universities (17CX05018, 17CX02056, 14CX02050A, 14CX02123A), Shandong Provincial Natural Science Foundation (ZR201702160196) and State Key Laboratory of Heavy Oil Processing Fund (SKLZZ-2017008).

References

[1] I. Maxwell, W. Stork, Hydrocarbon processing with zeolites, Surf. Sci. Catal.137 (2001) 747-819.

[2] S.J. Miller, New molecular sieve process for lube dewaxing by wax isomerization, Micropor. Mater. 2 (1994) 439-449.

[3] Y. Liu, W. Guo, X.S. Zhao, J. Lian, J. Dou, F. Kooli, Zeolite beta catalysts for n-C7

hydroisomerization, J. Porous Mat, 13 (2006) 359-364.

[4] Y. Izutsu, Y. Oku, Y. Hidaka, K. Yoshida, Y. Sasaki, Y. Sekine, E. Kikuchi, M. Matsukata, Synthesis and Characterization of Chromium-Added Pt/Beta Zeolite and its Catalytic Performance for n -Heptane Isomerization, Catal Lett, 143 (2013) 486-494.

[5] G. Burnens, C. Bouchy, E. Guillon, J. Martens, Hydrocracking reaction pathways of 2, 6, 10, 14-tetramethylpentadecane model molecule on bifunctional silica–alumina and ultrastable Y zeolite catalysts, J. Catal. 282 (2011) 145-154.

[6] J. Weitkamp, Isomerization of long-chain n-alkanes on a Pt/CaY zeolite catalyst, Ind. Eng. Chem. Res. 21 (1982) 550-558.

[7] A. Chica, A. Corma, Hydroisomerization of Pentane, Hexane, and Heptane for Improving the Octane Number of Gasoline, J. Catal. 187 (1999) 167-176.

[8] K.J. Chao, H.C. Wu, L.J. Leu, Hydroisomerization of light normal paraffins over series of platinum-loaded mordenite and beta catalysts, Appl. Catal. A. Gen. 143 (1996) 223-243.

[9] E. Blomsma, J.A. Martens, P.A. Jacobs, Mechanisms of Heptane Isomerization on Bifunctional Pd/H-Beta Zeolites, J. Catal. 159 (1996) 323-331.

[10] Z.B. Wang, A. Kamo, T. Yoneda, T. Komatsu, T. Yashima, Isomerization of n -heptane over Pt-loaded zeolite β catalysts, Appl. Catal. A. Gen. 159 (1997) 119-132.

[11] Y. Liu, W. Guo, X. Zhao, J. Lian, J. Dou, F. Kooli, Zeolite beta catalysts for n-C_7 hydroisomerization, J. Porous. Mat. 13 (2006) 359-364.

[12] A. Miyaji, T. Okuhara, Skeletal isomerization of n-heptane and hydroisomerization of benzene over bifunctional heteropoly compounds, Catal. Today. 81 (2003) 43-49.

[13] A. Miyaji, T. Echizen, K. Nagata, Y. Yoshinaga, T. Okuhara, Selective hydroisomerization of n-pentane to isopentane over highly dispersed Pd-$H_4SiW_{12}O_{40}/SiO_2$, J. Mol. Cata. A Chem. 201 (2003) 145-153.

[14] J. Wang, Z. Lin, S.Y. Han, M. Eum, C.W. Lee, 12-Tungstophosphoric Acid Supported on Dealuminated USY as a Catalyst for Hydroisomerization of n-Heptane, J. Ind. Eng. Chem., 9 (2003) 281-286.

[15] T.D. Pope, J.F. Kriz, M. Stanciulescu, J. Monnier, A study of catalyst formulations for isomerization of C_7 hydrocarbons, Appl. Catal. A Gen. 233 (2002) 45-62.

[16] A. Patrigeon, E. Benazzi, C. Travers, J.Y. Bernhard, Influence of the zeolite structure and acidity on the hydroisomerization of n -heptane, Catal.Today. 65 (2001) 149-155.

[17] K. Föttinger, K. Zorn, H. Vinek, Influence of the sulfate content on the activity of Pt containing sulfated zirconia, Appl. Catal. A. Gen. 284 (2005) 69-75.

[18] E. Iglesia, S.L. Soled, G.M. Kramer, Isomerization of Alkanes on Sulfated Zirconia: Promotion by Pt and by Adamantyl Hydride Transfer Species, J. Catal. 144 (1993) 238-253.

[19] M.A. Arribas, A. Martínez, Simultaneous isomerization of n-heptane and saturation of benzene over Pt/Beta catalysts, Catal. Today. 65 (2001) 117-122.

[20] P. Raybaud, A. Patrigeon, H. Toulhoat, The Origin of the C_7 -Hydroconversion Selectivities on Y, β, ZSM-22, ZSM-23, and EU-1 Zeolites, J. Catal. 197 (2001) 98-112.

[21] M.M.J. Treacy, J.M. Newsam, Two new three-dimensional twelve-ring zeolite frameworks of which zeolite beta is a disordered intergrowth, Nature. 332 (1988) 249-251.

[22] T. Matsuda, K. Watanabe, H. Sakagami, N. Takahashi, Catalytic properties of H_2-reduced MoO_3 and Pt/zeolites for the isomerization of pentane, hexane, and heptane, Appl. Catal. A. Gen. 242 (2003) 267-274.

[23] M. Tromp, J.A. van Bokhoven, M.T. Garriga Oostenbrink, J.H. Bitter, K.P. de Jong, D.C. Koningsberger, Influence of the Generation of Mesopores on the Hydroisomerization Activity and Selectivity of n-Hexane over Pt/Mordenite, J. Catal. 190 (2000) 209-214.

[24] S. van Donk, A. Broersma, O.L.J. Gijzeman, J.A. van Bokhoven, J.H. Bitter, K.P. de Jong, Combined Diffusion, Adsorption, and Reaction Studies of n-Hexane Hydroisomerization over Pt/H–Mordenite in an Oscillating Microbalance, J. Catal. 204 (2001) 272-280.

[25] J. Čejka, S. Mintova, Perspectives of micro/mesoporous composites in catalysis, Catal. Rev. Sci. Eng. 49 (2007) 457-509.

[26] J. Perez-Pariente, I. Diaz, J. Agundez, Organising Disordered Matter: Strategies for Ordering the Network of Mesoporous Materials, Cheminform, 36 (2005) 569–578.

[27] Y. Tao, H. Kanoh, L. Abrams, K. Kaneko, Mesopore-modified zeolites:preparation, characterization, and applications, Chem. Rev. 106 (2006) 896-910.

[28] K. Egeblad, C.H. Christensen, M. Kustova, C.H. Christensen, Templating Mesoporous Zeolites, Chem. Mater. 20 (2008) 946-960.

[29] M. Ogura, Towards Realization of a Micro- and Mesoporous Composite Silicate Catalyst, Catal. Surv. Asia. 12 (2008) 16-27.

[30] K. Egeblad, C.H. Christensen, M. Kustova, C.H. Christensen, Templating Mesoporous Zeolites, Chem. Materials. 20 (2008) 946-960.

[31] Y. Liu, T.J. Pinnavaia, Aluminosilicate Mesostructures with Improved Acidity and Hydrothermal Stability, Cheminform, 12 (2002) 3179-3190.

[32] Y. Xia, R. Mokaya, On the synthesis and characterization of ZSM-5/MCM-48 aluminosilicate composite materials, J. Mate. Chem. 14 (2004) 863-870.

[33] Y.S. Ooi, R. Zakaria, A.R. Mohamed, S. Bhatia, Synthesis of composite material MCM-41/Beta and its catalytic performance in waste used palm oil cracking, Appl. Catal. A. Gen. 274 (2004) 15-23.

[34] S. Wang, T. Dou, Y. Li, Y. Zhang, X. Li, Z. Yan, A novel method for the preparation of MOR/MCM-41 composite molecular sieve, Catal. Commun. 6 (2005) 87-91.

[35] H. Zhang, Y. Li, Preparation and characterization of Beta/MCM-41composite zeolite with a stepwise-distributed pore structure, Powder. Technol. 183 (2008) 73-78.

[36] Q.S.Huo, D.I.Margolese, G.D.Stucky, Surfactant Control of Phases in the Synthesis of Mesoporous Silica-Based Materials, Chem. Mater. 8 (1996) 1147-1160.

[37] S.J. Gregg, K.S.W. Sing, Adsorption, surface area, and porosity, Academic Pr.*1982.

[38]C.A. EMEIS, ChemInform Abstract: Determination of Integrated Molar Extinction Coefficients for IR Absorption Bands of Pyridine Adsorbed on Solid Acid Catalysts, J. Catal. 141 (1993)347-354.

[39] J. Perez-Pariente, J. A. Martens, P. A. Jacobs, Crystallization mechanism of zeolite beta from $(TEA)_2O$, Na_2O and K_2O containing aluminosilicate gels, Appl. Catal. 31 (1987) 35-64.

[40] J. Perez-Pariente, J.A. Martens, P.A. Jacobs, Factors affecting the synthesis efficiency of zeolite BETA from aluminosilicate gels containing alkali and tetraethylammonium ions, Zeolites. 8 (1988) 46-53.

[41] I.I. Ivanova, E.E. Knyazeva, Micro-mesoporous materials obtained by zeolite recrystallization: synthesis, characterization and catalytic applications, Chem. Soc.Rev. 42 (2013) 3671-3688.

[42] H. Xu, J. Guan, S. Wu, Q. Kan, Synthesis of Beta/MCM-41 composite molecular sieve with high hydrothermal stability in static and stirred condition, J. Colloid. Interf. Sci. 329 (2009) 346-350.

[43] S. Inagaki, M. Ogura, T. Inami, Y. Sasaki, E. Kikuchi, M. Matsukata, Synthesis of MCM-41-type mesoporous materials using filtrate of alkaline dissolution of ZSM-5 zeolite, Micropor. Mesopor. Mat. 74 (2004) 163-170.

[44] C.T. Kresge, M.E. Leonowicz, W.J. Roth, J.C. Vartuli, J.S. Beck, Ordered mesoporous molecular sieves synthesized by a liquid-crystal template mechanism, Nature. 359 (1992) 710-712.

[45] J.S. Beck, J.C. Vartuli, W.J. Roth, M.E. Leonowicz, C.T. Kresge, K.D. Schmitt, C.T.W. Chu, D.H. Olson, E.W. Sheppard, S.B. McCullen, J.B. Higgins, J.L. Schlenker, A new family of mesoporous molecular sieves prepared with liquid crystal templates, J. Am. Chem. Soc. 114 (1992) 10834-10843.

[46] K.A. Cychosz, R. Guillet-Nicolas, J. García-Martínez, M. Thommes, Recent advances in the textural characterization of hierarchically structured nanoporous materials, Chem. Soc. Rev. 46 (2017) 389.

[47] M.A. Camblor, A. Corma, S. Valencia, Characterization of nanocrystalline zeolite Beta, Micropor. Mesopor. Mat. 25 (1998) 59-74.

[48] S.A. Bagshaw, N.I. Baxter, D.R.M. Brew, C.F. Hosie, Y. Nie, S. Jaenicke, C.G. Khuan, Highly ordered mesoporous MSU-SBEA/zeolite Beta composite material, J. Mate. Chem. 16 (2006) 2235-2244.

[49] V. Umamaheswari, M. Palanichamy, V. Murugesan, Isopropylation of m-Cresol over Mesoporous Al–MCM-41 Molecular Sieves, J. Catal. 210 (2002) 367-374.

[50] J. Perez-Pariente, J.A. Martens, P.A. Jacobs, Crystallization mechanism of zeolite beta from $(TEA)_2O$, Na_2O and K_2O containing aluminosilicate gels, Appl. Catal. 31 (1987) 35-64.

[51] T. Lopez, J. Navarrete, R. Gomez, O. Novaro, F. Figueras, H. Armendariz, Preparation of sol-gel sulfated ZrO_2 SiO_2 and characterization of its surface acidity, Appl. Catal. A. Gen. 125 (1995) 217–232.

[52] J.A. Wang, X. Bokhimi, O. Novaro, T. López, F. Tzompantzi, R. Gómez, J. Navarrete, M.E. Llanos, E. López-Salinas, Effects of structural defects and acid–basic properties on the activity and selectivity of isopropanol decomposition on nanocrystallite sol-gel alumina catalyst, J. Mol. Catal. A- Chem. 137 (1999) 239-252.

[53] D. Srinivas, R. Srivastava, P. Ratnasamy, Transesterifications over titanosilicate molecular sieves, Catal. Today. 96 (2004) 127-133.

[54] L.F. Chen, L.E. Noreña, J. Navarrete, J.A. Wang, Improvement of surface acidity and structural regularity of Zr-modified mesoporous MCM-41, Materials Chem. Phys. 97 (2006) 236-242.

[55] D. Liu, X.Y. Quek, S. Hu, L. Li, M.L. Hui, Y. Yang, Mesostructured TUD-1 supported molybdophosphoric acid (HPMo/TUD-1) catalysts for n-heptane hydroisomerization, Catal. Today. 147 (2009) S51-S57.

[56] D. Liu, S. Hu, R. Lau, A. Borgna, G.L. Haller, Y. Yang, Hydroconversion of n-heptane over Pt/Al-MCM-41 mesoporous molecular sieves, Chem. Eng. J. 151 (2009) 308-318.

[57] W. Guo, L. Huang, P. Deng, Z. Xue, Q. Li, Characterization of Beta/MCM-41 composite molecular sieve compared with the mechanical mixture, Micropor. Mesopor. Mat. 44 (2001) 427-434.

[58] M.L. Maloncy, T. Maschmeyer, J.C. Jansen, Technical and economical evaluation of a zeolite membrane based heptane hydroisomerization process, Chem. Eng. J. 106 (2005) 187-195.

[59] Z.B. Wang, A. Kamo, T. Yoneda, T. Komatsu, T. Yashima, Isomerization of n-heptane over Pt-loaded zeolite β catalysts, Appl. Catal. A. Gen. 159 (1997) 119-132.

[60] A. Aerts, W. Huybrechts, S.P. Kremer, C.E. Kirschhock, E. Theunissen, I.A. Van, J.F. Denayer, G.V. Baron, J.W. Thybaut, G.B. Marin, n-Alkane hydroconversion on Zeogrid and colloidal ZSM-5 assembled from aluminosilicate nanoslabs of MFI framework type, Chem. Commun. 9 (2003) 1888.

[61] S.H. Sie, Progress of quantitative micro-PIXE applications in geology and mineralogy, Nucl. Instrum. Meth. B. 75 (1993) 403-410.

[62] M. Guisnet, F. Alvarez, G. Giannetto, G. Perot, Hydroisomerization and hydrocracking of n-heptane on Pth zeolites. Effect of the porosity and of the distribution of metallic and acid sites, Catal. Today. 1 (1987) 415-433.

[63] A. Patrigeon, E. Benazzi, C. Travers, J.Y. Bernhard, Influence of the zeolite structure and acidity on the hydroisomerization of n-heptane, Catal. Today. 65 (2001) 149-155.

[64] A. Lugstein, A. Jentys, H. Vinek, Hydroconversion of n-heptane over bifunctional HZSM5 zeolites influence of the metal concentration and distribution on the activity and selectivity, Appl. Catal. A. Gen. 166 (1998) 29-38.

[65] S. Gopal, P.G. Smirniotis, Factors affecting isomer yield for n-heptane hydroisomerization over as-synthesized and dealuminated zeolite catalysts loaded with platinum, J. Catal. 225 (2004) 278-287.

[66] T.L.M. Maesen, M. Schenk, T.J.H. Vlugt, B. Smit, Differences between MFI- and MEL-Type Zeolites in Paraffin Hydrocracking, J. Catal. 203 (2001) 281-291.

[67] Y. Hu, X. Wang, X. Guo, S. Li, S. Hu, H. Sun, L. Bai, Effects of channel structure and acidity of molecular sieves in hydroisomerization of n-octane over bi-functional catalysts, Catal. Lett. 100 (2005) 59-65.

[68] R. Roldán, F.J. Romero, C. Jiménez-Sanchidrián, J.M. Marinas, J.P. Gómez, Influence of acidity and pore geometry on the product distribution in the hydroisomerization of light paraffins on zeolites, Appl. Catal. A. Gen. 288 (2005) 104-115.

[69] J. Pérez-Ramírez, D. Verboekend, A. Bonilla, S. Abelló, Zeolite Catalysts with Tunable Hierarchy Factor by Pore‐Growth Moderators, Adv. Funct. Mater.19 (2009) 3972-3979.

[70] J.C. Groen, W. Zhu, S. Brouwer, S.J. Huynink, F. Kapteijn, J.A. Moulijn, J. Perez-Ramirez, Direct Demonstration of Enhanced Diffusion in Mesoporous ZSM‐5 Zeolite Obtained via Controlled Desilication, J. Am. Chem. Soc. 38 (2007) 355-360.

[71] L. Guo, X. Bao, Y. Fan, G. Shi, H. Liu, D. Bai, Impact of cationic surfactant chain length during SAPO-11 molecular sieve synthesis on structure, acidity, and n-octane isomerization to di-methyl hexanes, J. Catal. 294 (2012) 161-170.

[72] P. Liu, J. Wang, X. Zhang, R. Wei, X. Ren, Catalytic performances of dealuminated Hβ zeolite supported Pt catalysts doped with Cr in hydroisomerization of n-heptane, Chem. Eng. J. 148 (2009) 184-190.

[73] R. Yadav, A. Sakthivel, Silicoaluminophosphate molecular sieves as potential catalysts for hydroisomerization of alkanes and alkenes, Appl. Catal. A. Gen. 481 (2014) 143-160.

[74] Y. Hu, X. Wang, X. Guo, S. Li, S. Hu, H. Sun, B. Liang, Effects of channel structure and acidity of molecular sieves in hydroisomerization of n -octane over bi-functional catalysts, Catal. Lett. 100 (2005) 59-65.

[75] Y. Bi, G. Xia, W. Huang, H. Nie, Hydroisomerization of long chain n-paraffins: the role of the acidity of the zeolite, Rsc. Adv. 5 (2015) 99201-99206.

[76] G. Kinger, H. Vinek, n-Nonane hydroconversion on Ni and Pt containing HMFI, HMOR and HBEA, Appl. Catal. A. Gen. 218 (2001) 139-149.

[77] W. Zhang, P.G. Smirniotis, Effect of Zeolite Structure and Acidity on the Product Selectivity and Reaction Mechanism for n-Octane Hydroisomerization and Hydrocracking, J. Catal. 182 (1999) 400–416.

[78] K.C. Park, S.K. Ihm, Comparison of Pt/zeolite catalysts for n-hexadecane hydroisomerization, Appl. Catal. A. Gen. 203 (2000) 201-209.

[79] G. Talebi, M. Sohrabi, S.J. Royaee, R.L. Keiski, M. Huuhtanen, H. Imamverdizadeh, Synthesis and activity measurement of the some bifunctional platinum loaded Beta zeolite catalysts for n-heptane hydroisomerization, J. Ind. Eng. Chem. 14 (2008) 614-621.

[80] X. Yang, J.A. Wang, L. Chen, S.P.R. Sebastian, A.M. Robledo, Heteropolyacid grafted Pt/Si-MCM-41 catalyst for C_7 skeletal isomerization, Catal. Commun. 28 (2012) 202-206.

[81] P. Liu, J. Ren, Y. Sun, Influence of template on Si distribution of SAPO-11 and their performance for n-paraffin isomerization, Micropor. Mesopor. Mater. 114 (2008) 365-372.

[82] X. Yang, J.A. Wang, L. Chen, S.P.R. Sebastian, A.M. Robledo, Heteropolyacid grafted Pt/Si-MCM-41 catalyst for C_7 skeletal isomerization, Catal. Commun. 28 (2012) 202-206.